Fermi Surface of the Electron-doped Cuprate Superconductor $Nd_{2-x}Ce_xCuO_4$ Probed by High-Field Magnetotransport

M. V. Kartsovnik[1], T. Helm[1], C. Putzke[2], F. Wolff-Fabris[2], I. Sheikin[3], S. Lepault[4], C. Proust[4], D. Vignolles[4], N. Bittner[1], W. Biberacher[1], A. Erb[1], J. Wosnitza[2], and R. Gross[1,51,2,3,4,5]

[11] *Walther-Meißner-Institut, Bayerische Akademie der Wissenschaften, Walther-Meißner-Str. 8, D-85748 Garching, Germany*

[22] *Hochfeld-Magnetlabor Dresden, Forschungszentrum Dresden-Rossendorf, Bautzner Landstr. 400, D-01328 Dresden, Germany*

[33] *Laboratoire National des Champs Magnétiques Intenses, CNRS, 25 rue des Martyrs, B.P. 166, F-38042 Grenoble, France*

[44] *Laboratoire National des Champs Magnétiques Intenses, (CNRS, INSA, UJF, UPS), F-31400 Toulouse, France*

[55] *Physik-Department, Technische Universität München, James-Franck-Str., D-85748 Garching, Germany**

Abstract

We report on the study of the Fermi surface of the electron-doped cuprate superconductor $Nd_{2-x}Ce_xCuO_4$ by measuring the interlayer magnetoresistance as a function of the strength and orientation of the applied magnetic field. We performed experiments in both steady and pulsed magnetic fields on high-quality single crystals with Ce concentrations of $x = 0.13$ to 0.17. In the overdoped regime of $x > 0.15$ we found both semiclassical angle-dependent magnetoresistance oscillations (AMRO) and Shubnikov-de Haas (SdH) oscillations. The combined AMRO and SdH data clearly show that the appearance of fast SdH oscillations in strongly overdoped samples is caused by magnetic breakdown. This observation provides clear evidence for a reconstructed multiply-connected Fermi surface up to the very end of the overdoped regime at $x \simeq 0.17$. The strength of the superlattice potential responsible for the reconstructed Fermi surface is found to decrease with increasing doping level and likely vanishes at the same carrier concentration as superconductivity, suggesting a close relation between translational symmetry breaking and superconducting pairing. A detailed analysis of the high-resolution SdH data allowed us to determine the effective cyclotron mass and Dingle temperature, as well as to estimate the magnetic breakdown field in the overdoped regime.

PACS numbers: 74.72.Ek, 71.18.+y, 72.15.Gd, 74.25.Jb

INTRODUCTION

Electronic correlations and the resulting ordering instabilities are central issues in the long-standing problem of high-temperature superconductivity in copper oxides. To elucidate them, the exact knowledge of the Fermi surface and its evolution with doping is of crucial importance. High-field magnetotransport is known as one of the most powerful tools for studying Fermi surfaces of conventional metals [1, 2]. It has recently proved very efficient also in the case of cuprate superconductors. A breakthrough in the Fermiology of hole-doped cuprates was made by the observation of semiclassical angle-dependent magnetoresistance oscillations (AMRO) [3, 4] and quantum oscillations of the resistance, the Shubnikov-de Haas (SdH) effect [5–8].

On the strongly overdoped side of the phase diagram of hole-doped cuprate superconductors, both the semiclassical AMRO [3] and quantum oscillations of the resistance [8] have been found for the compound $Tl_2Ba_2CuO_{6+\delta}$. These experiments provided evidence for a large cylindrical Fermi surface, as expected from band-structure calculations [9, 10] and angle-resolved photoemission spectroscopy (ARPES) [11]. In contrast, for underdoped $YBa_2Cu_3O_{6.5}$ [5, 12, 13] and $YBa_2Cu_4O_8$ [6, 7] slow SdH and de Haas-van Alphen (dHvA) oscillations were found, indicating a reconstruction of the Fermi surface. These observations reveal substantial disagreements with ARPES results [14] and are controversially interpreted at present, see e.g. Refs. [12, 15–25]. The electron-doped cuprates $Ln_{2-x}Ce_xCuO_4$ (Ln = Nd, Pr, Sm) have a number of advantages for high-field Fermi surface studies, as compared to hole-doped cuprates. Due to their lower critical fields, superconductivity can easily be suppressed and the normal state is accessed for any doping level even at the lowest temperatures by applying a magnetic field $B \gtrsim 10\,\mathrm{T}$ (perpendicular to CuO_2 layers). Moreover, the Fermi surface is expected to be simple: there are neither CuO chains nor any bilayer potential and the magnetic superstructure, established in underdoped compounds, is commensurate. Another important advantage is that, in contrast to most of the hole-doped cuprates, the entire doping range, from the undoped insulating up to the strongly overdoped metallic (superconducting) phase, can be covered using one and the same compound with just slightly different Ce concentrations [see Fig. 1(a)].

We have recently reported on SdH oscillations in $Nd_{2-x}Ce_xCuO_4$ (NCCO) single crystals with Ce concentrations corresponding to nearly optimal doping ($x = 0.15$) and to over-

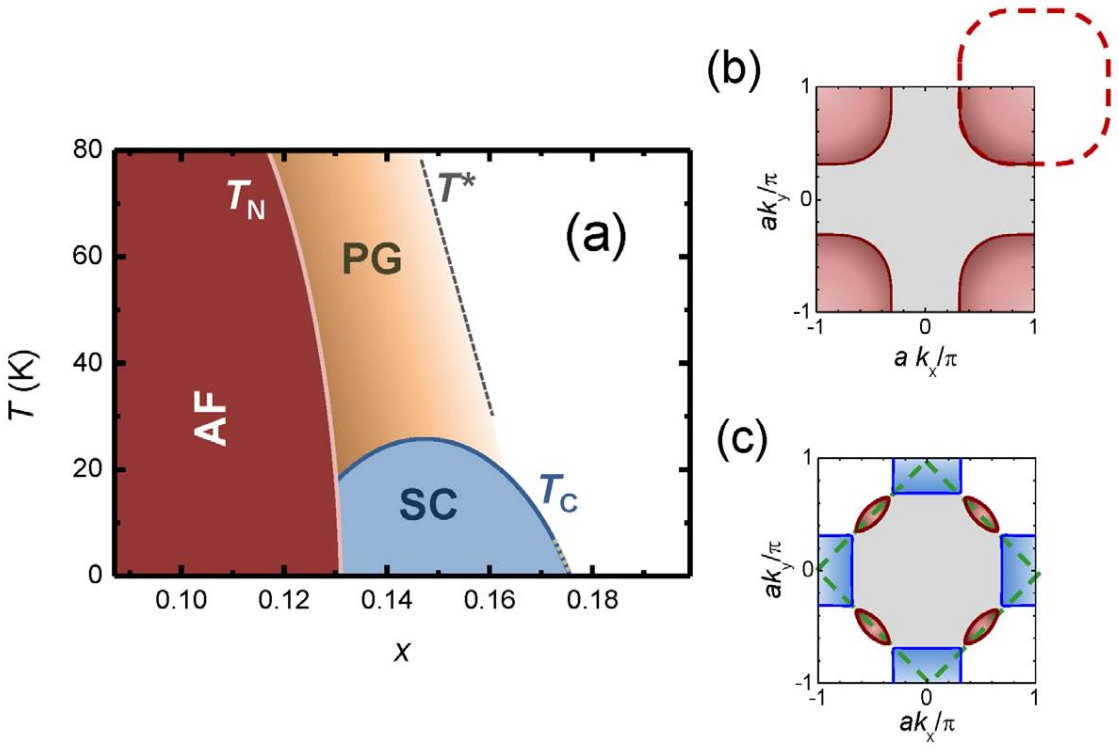

FIG. 1. (a) Schematic phase diagram of $Nd_{2-x}Ce_xCuO_4$ including the normal conducting, the pseudogap (PG), the antiferromagnetic insulating (AF), and the superconducting (SC) state together with the corresponding transition temperatures T^*, T_N, and T_c depending on the Ce concentration x. (b) The Fermi surface of NCCO in the absence of a superlattice potential is represented by a single hole-like cylinder centered at the corner of the Brillouin zone and slightly warped in the direction perpendicular to CuO_2 layers. In a strong magnetic field charge carriers move on large closed orbits (red dashed line) encircling the area corresponding to the fast SdH oscillations. (c) The Fermi surface, reconstructed due to a $(\pi/a, \pi/a)$ superlattice potential, consists of electron (blue) and hole (dark red) pockets. The size of the small hole pockets is consistent with the frequency of slow oscillations observed for the optimal, $x = 0.15$, and slightly overdoped, $x = 0.16$, compositions [26].

doped compositions ($x = 0.16$ and 0.17) [26]. For the highest doping level, $x = 0.17$, corresponding to the very end of the superconducting region on the overdoped side, fast SdH oscillations were found. In complete analogy with the hole-overdoped $Tl_2Ba_2CuO_{6+\delta}$ (Tl2201) compound, the oscillation frequency, $F_{\rm fast} \approx 11$ kT, reveals a large cyclotron orbit on the cylindrical Fermi surface centered at the corner of the Brillouin zone, as shown in

Fig. 1(b), and occupying $\approx 41\%$ of the first Brillouin zone. This result is in full agreement with band-structure calculations [27] and ARPES experiments [28, 29]. However, on crystals with the Ce concentration reduced by just 1% no fast oscillations have been found. Instead, oscillations with a much lower frequency have been observed for $x = 0.16$ and 0.15. These slow oscillations indicate a reconstruction of the Fermi surface caused by a translational symmetry breaking in the electronic system. Most remarkably, the transformation to a reconstructed Fermi surface occurs deep in the overdoped regime. While this result is in good agreement with the Hall effect measurements on NCCO crystals [30] and $Pr_{2-x}Ce_xCuO_4$ thin films [31], it is obviously inconsistent with the conclusions of ARPES [28, 29] and neutron-scattering studies [29].

An important issue to be clarified is the exact origin of the Fermi surface reconstruction which was revealed by the SdH oscillations in our overdoped NCCO samples. It was proposed [26, 32] to be caused by a $(\pi/a, \pi/a)$ superlattice potential (a is the lattice constant within the CuO_2 plane) which is known to exist in undoped and underdoped NCCO [28, 33]. Indeed, the frequency of the slow SdH oscillations, $F_{\rm slow} \approx 300\,\mathrm{T}$, is consistent with the size of small hole pockets, which should be formed around $(\pm\pi/2a, \pm\pi/2a)$ due to such ordering [see Fig. 1(c)]. On the other hand, no indication of electron pockets, required by the proposed reconstructed Fermi surface topology, were found in the SdH spectra. Obviously, additional work is needed for further verifying the reconstruction scenario. For example, it would be desirable to determine not only the size but also the shape of the Fermi pockets. Towards this end, the study of semiclassical AMRO is a very efficient tool. AMRO have been widely used for mapping in-plane Fermi surfaces of organic conductors [34] and other layered systems such as Sr_2RuO_4 [35] and intercalated graphite [36]. This effect has a geometrical origin and is directly related to the shape of a weakly warped cylindrical Fermi surface [3, 37–39]. As mentioned above, AMRO already have been observed in hole-overdoped $Tl_2Ba_2CuO_{6+\delta}$ (Tl2201) samples [3, 4] and successfully used for extracting the shape of the three-dimensional Fermi surface as well as for evaluating the scattering anisotropy.

Very recently, we have also found features characteristic of AMRO in the angle-dependent interlayer magnetoresistance of overdoped NCCO [40]. Although the magnitude of these features observed in applied magnetic fields up to 28 T was too low for a reliable quantitative analysis, they provided an important argument for the existence of magnetic-breakdown orbits on the Fermi surface. This magnetic breakdown scenario was further supported by

the observation of two frequencies in the SdH spectrum obtained for strongly overdoped ($x = 0.17$) NCCO crystals [40].

Here, we present new data on the interlayer magnetoresistance of NCCO single crystals studied as a function of the orientation and strength of the applied magnetic field at Ce concentrations between $x = 0.16$ and 0.17, corresponding to the overdoped regime of the phase diagram [see Fig. 1(a)]. Our studies confirm the existence of AMRO and reveal magnetic-breakdown quantum oscillations at compositions down to $x = 0.16$.

EXPERIMENTAL TECHNIQUES

Single crystals of NCCO were grown by the traveling solvent floating zone (TSFZ) method and thermally treated in pure argon to remove interstitial oxygen and release internal strain. The crystals were thoroughly tested by x-ray diffraction, magnetic and resistive measurements. The best samples, with the lowest doping inhomogeneity (typically within 0.25%) and the largest (high-to-low temperature) resistance ratios, see Fig. 2(a), were selected for the high-field experiments. Details of crystal preparation and characterization are presented elsewhere [41].

The resistance of the samples was measured out-of-plane, that is in the direction perpendicular to the conducting CuO_2 layers, for two reasons. First, for the angle-dependent magnetoresistance studies: the AMRO phenomenon mentioned in Section is an inherent property of the interlayer magnetoresistance and should be much more pronounced in this configuration [34, 42]. Second, due to the high resistivity anisotropy, $\sim 10^3$, the interlayer resistance value is usually much higher than the in-plane resistance and, hence, easier to measure. Taking the advantage of the TSFZ technique[**?**], we were able to further increase the signal by optimizing the shape of the crystal cut out of the as-grown rod. Given the room-temperature resistivity of NCCO in the range 3 to $6\,\Omega\,\mathrm{cm}$, depending on the doping level, and the typical sample dimensions, about $0.3 \times 0.3 \times 1\,\mathrm{mm}^3$ with the largest dimension along the c-axis, we could obtain a resistance of $300 - 600\,\Omega$ at room temperature and $30 - 100\,\Omega$ at low temperatures. For some batches we had to decrease the sample thickness to avoid crystal inhomogeneity. In those cases the low-temperature resistance values were $\sim 1 - 10\,\Omega$. These values are still quite convenient and can be measured accurately.

Fig. 2(b) shows a NCCO crystal prepared for high-magnetic-field measurements. For

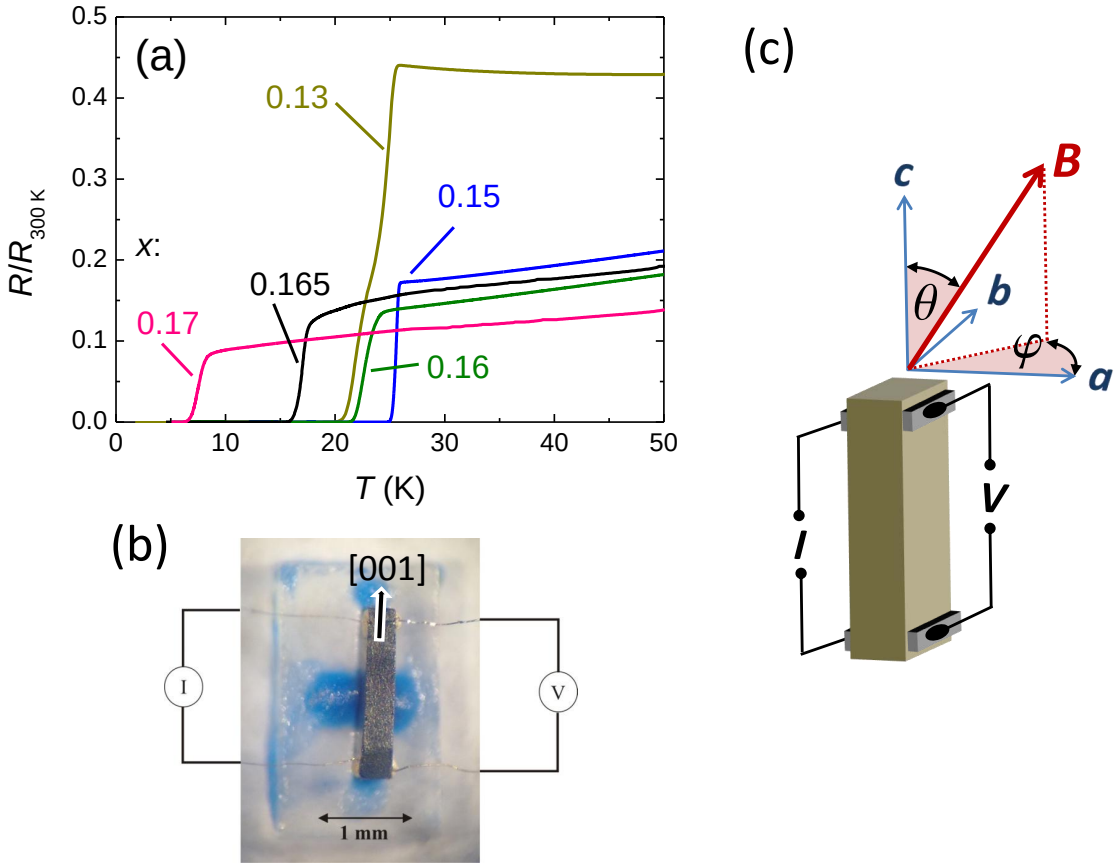

FIG. 2. (a) Temperature-dependent interlayer resistance, normalized to its room-temperature value, for typical $Nd_{2-x}Ce_xCuO_4$ crystals studied in this work. The labels 0.13 to 0.17 indicate the Ce concentration x, which is considered to be equal to the electron doping level [41]. (b) Photograph of a NCCO crystal with current (I) and voltage (V) leads mounted on a sapphire plate and prepared for high-field measurements. Note that the largest dimension of the sample is along the c-axis. (c) Schematic view of the experimental geometry. The current is applied parallel to the c-axis; angles θ and φ define the orientation of the magnetic field with respect to the crystal axes.

voltage and current leads, annealed 20 μm Pt wires were attached using either Dupont 4929 silver paste or Epo-Tek H20E conducting epoxy. The latter provided the most reliable contacts with the lowest resistance. Due to their highly anisotropic susceptibility caused by the magnetic moments of the Nd^{3+} ions, NCCO crystals experience a very strong torque in a tilted magnetic field. Therefore, for our experiments we firmly glued the samples to a sapphire plate by Stycast 2860 FT (blue color), as shown in Fig. 2(b). The plate was then

fixed by the same epoxy to an appropriate sample holder.

The angle-dependent magnetoresistance was measured in steady fields up to 28 and 34 T provided by the 20 MW resistive magnet at the LNCMI-Grenoble. The samples were mounted onto a home-made two-axes sample rotator allowing an *in situ* rotation at a fixed B, at temperatures between 50 and 1.4 K. The resistance was measured as a function of polar angle θ between the field direction and the crystallographic c-axis for different fixed azimuthal angles φ, as shown in Fig. 2(c). SdH oscillations were studied with the magnetic field applied parallel to the c-axis. These experiments were done in pulsed fields provided by the Dresden and Toulouse high-field facilities as well as in steady fields at Grenoble.

ANGLE-DEPENDENT SEMICLASSICAL MAGNETORESISTANCE

Fig. 3 shows examples of the angle-dependent interlayer magnetoresistance of NCCO for different doping levels, recorded at high magnetic fields and $T = 1.5\,\mathrm{K}$. At field directions almost parallel to the conducting CuO_2 plane (i.e. around $\theta = \pm 90^\circ$) the resistance drops down due to the onset of superconductivity. Outside the superconducting angular range, the $R(\theta)$ curves exhibit different shapes, depending on Ce concentration. The typical behavior of underdoped samples is shown in Fig. 3(a). The resistance is maximum for the field direction perpendicular to the CuO_2 planes, i.e. for $\theta = 0^\circ$, and then gradually decreases at tilting the field towards the in-plane direction, until superconductivity sets in at high tilt angles [$|\theta| > 70^\circ$ for $x = 0.13$, $T = 1.5$ K, and $B = 28$ T, as shown in Fig. 3(a)]. The dome-like shape of the $R(\theta)$ curve centered at $\theta = 0^\circ$ is opposite to what one expects for a typical layered metal. There, the magnetoresistance generally increases with increasing $|\theta|$ [34]. The anomalous θ-dependence obtained for NCCO is almost insensitive to the azimuthal orientation of the applied field, that is, to the angle φ. This suggests that it is determined solely by the out-of-plane field component. Such behavior is similar to what was observed in some organic layered metals and associated with incoherent interlayer charge transfer (for a recent discussion, see [43]). In addition, the $R(\theta)$ dependence taken at $\varphi = 0^\circ$ exhibits a clear hysteresis with respect to the rotation direction at $|\theta| \geq 6^\circ$. This hysteretic behavior is most likely related to a field-induced reorientation of ordered spins. Indeed, recent reports on the in-plane field rotation [44, 45] point to a significant role of spin ordering in the magnetoresistance of underdoped NCCO. Notably, in our experiments signatures of spin

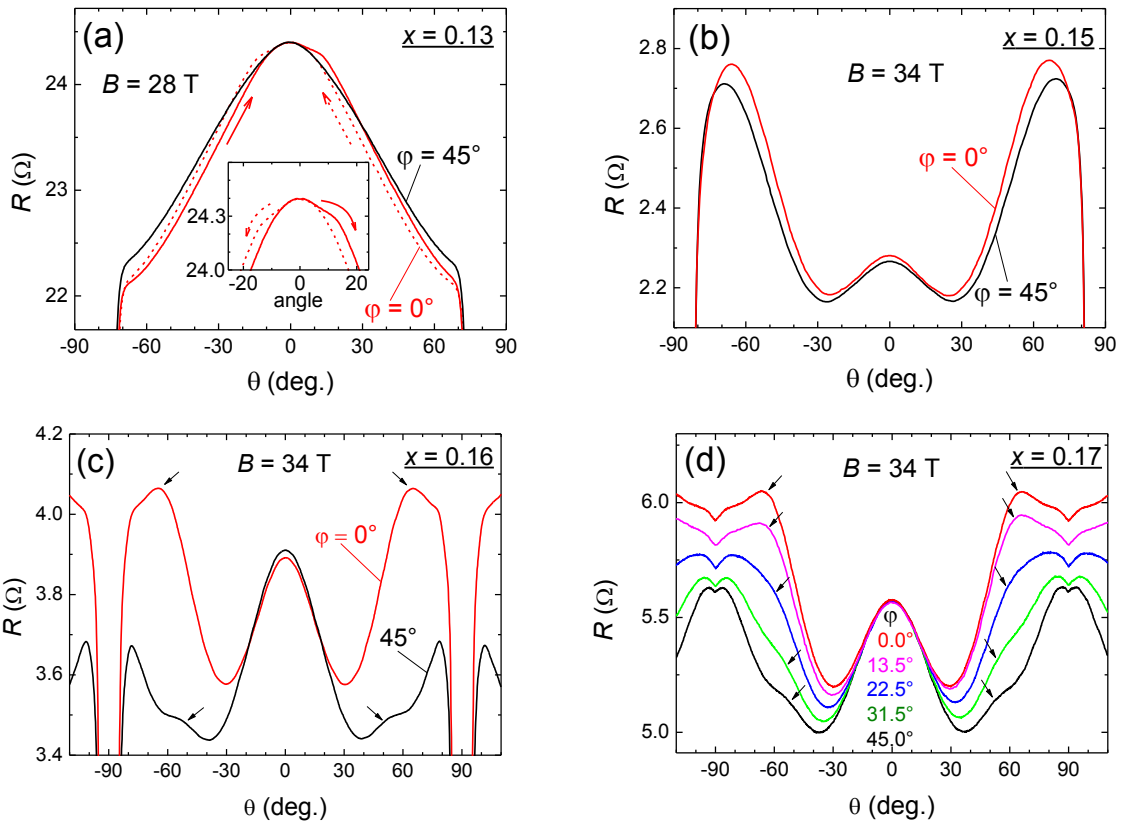

FIG. 3. Angle-dependent interlayer magnetoresistance of $Nd_{2-x}Ce_xCuO_4$ single crystals with doping level $x = 0.13$ (a), 0.15 (b), 0.16 (c), and 0.17 (d) recorded at $T = 1.5\,\mathrm{K}$ and applied magnetic fields of 28 T (a) and 34 T (b) to (d). The overdoped samples (c) and (d) exhibit AMRO features (marked by arrows) with their θ positions being dependent on the azimuthal angle φ.

ordering are present even in the superconducting compound with $x = 0.13$. Further work is necessary for clarifying the detailed mechanism responsible for coupling the interlayer magnetoresistance to electron spins.

As we increase the Ce concentration to the optimal and, further on, to the overdoped regime, the anomalous contribution to the magnetoresistance weakens, giving way to the conventional behavior associated with the orbital effect of the applied magnetic field on the charge carriers. This causes a positive, φ-dependent slope $dR/d|\theta| > 0$ of the angular dependence $R(\theta)$ over an extended angular range $30^\circ \lesssim |\theta| \lesssim 80^\circ$, as shown in Fig. 3(b) to (d) for samples with $x = 0.15$, 0.16, and 0.17. The most interesting feature in the overdoped regime is a shallow hump (marked by arrows) superposed on the monotonic slope at $|\theta| \simeq 53-62^\circ$, depending on φ. The sensitivity of the angular position of the hump to the

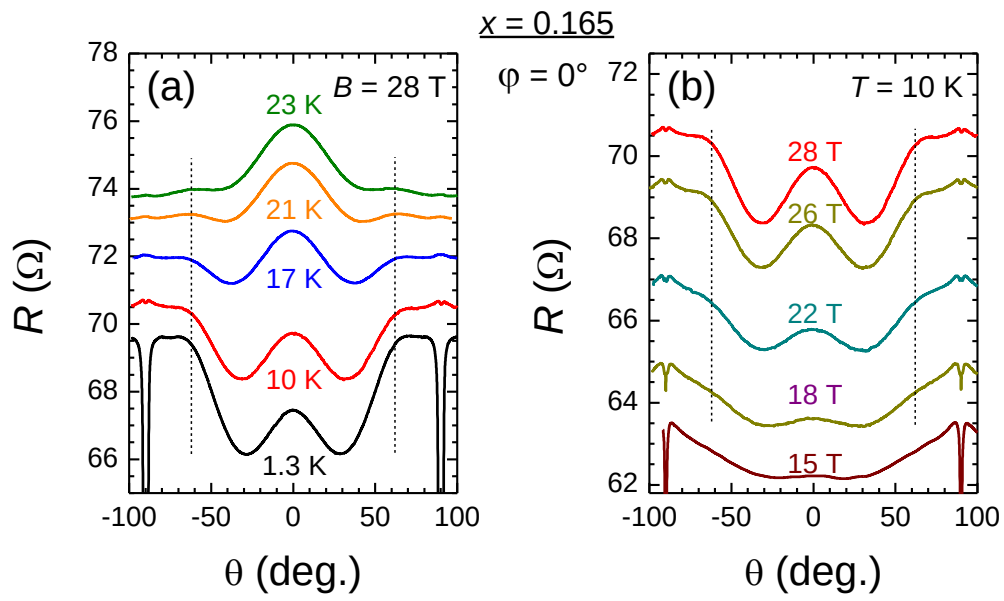

FIG. 4. Angle-dependent magnetoresistance of a $Nd_{2-x}Ce_xCuO_4$ single crystal with $x = 0.165$ taken at different temperatures (a) and different magnetic field strengths (b). One can see that the AMRO positions (marked by vertical dashed lines) are independent of T and B.

azimuthal orientation and its independence of temperature and the magnetic field strength, as is shown in Fig. 4, clearly point to the geometrical origin of this feature. Therefore, we attribute this hump-like feature to the AMRO effect.

The $R(\theta)$ curves in Fig. 3(c),(d) are qualitatively similar to the angle-dependent magnetoresistance of the hole-overdoped cuprate Tl2201 [3, 4], which also exhibits a local maximum around $\theta = 0°$ and a shoulder at $|\theta| \simeq 30 - 40°$. In Tl2201 having the same body-centered tetragonal crystal symmetry, the entire angular dependence can be nicely described within the semiclassical Boltzmann transport model with a **k**-dependent scattering time [4, 46]. In particular, both the central hump and the side feature come from the AMRO effect of the slightly warped large Fermi cylinder centered at the corner of the Brillouin zone. By analogy, it is tempting to consider our data on NCCO as a manifestation of the unreconstructed large Fermi cylinder, as in Fig. 1(b). However, the situation seems to be more intricate. By contrast to the case of Tl2201, the central ($\theta = 0°$) hump is much more pronounced, as compared to the side features. Furthermore, at odds with what is expected from an AMRO peak, it does not diminish at increasing the temperature. Instead, it develops in size and becomes a dominating feature in the angular dependence above $\sim 20\,\mathrm{K}$, as shown, e.g., in Fig. 4(a)

for a sample with $x = 0.165$. The 21 and 23 K curves in this Figure rather resemble the $R(\theta)$ dependence in the underdoped, $x = 0.13$ NCCO, c.f. Fig. 3(a). It is, therefore, likely [40] that, at least at elevated temperatures, the central hump originates from a remnant of the anomalous, presumably incoherent, interlayer transport channel rather than from the conventional AMRO effect.

The superposition of the conventional orbital and anomalous contributions to the $R(\theta)$ dependence makes it problematic for a quantitative analysis. However, already at the present stage, we can assert that the Fermi surface giving rise to the AMRO is the same in the doping interval from $x = 0.16$ to 0.17. This is evidenced by the similarity of the AMRO features in Fig. 3(c),(d) and Fig. 4, as well as by their angular positions shown in Fig. 5. Having in mind the strong difference between the quantum-oscillation spectra reported for $x = 0.16$ and 0.17 [26], one is lead to the conclusion that the large cyclotron orbit, indistinguishable from that on the original Fermi cylinder shown in Fig. 1(b), and the small orbit corresponding to hole pockets of the reconstructed Fermi surface [see Fig. 1(c)] should coexist at one and the same composition. Indeed, this was confirmed by the observation of both SdH frequencies in the strongly overdoped ($x = 0.17$) NCCO crystal [40]. In Section , we present further data on quantum oscillations which provides clear evidence for magnetic breakdown to take place also at lower doping down to $x = 0.16$.

We note that for $x = 0.15$ the $R(\theta)$ dependence presented in Fig. 3(b) does not show clear AMRO features up to $B = 34$ T. This seems to favor the scenario of the large magnetic breakdown orbit being responsible for the AMRO: with decreasing x from 0.16 to 0.15, the superlattice potential is enhanced, leading to an increase of the energy gap between different parts of the reconstructed Fermi surface and thereby impeding magnetic breakdown. The suppression of magnetic breakdown could be a reason for the absence of the AMRO at $x = 0.15$, if the latter were caused by the breakdown orbit. On the other hand, one should keep in mind that the composition $x = 0.15$ is closer to the underdoped regime, in which the magnetoresistance is dominated by the anomalous incoherent mechanism. This should also suppress the AMRO effect even if it is caused by small orbits on the reconstructed Fermi surface. In this context, it would be interesting to study the angle-dependent magnetoresistance of the $x = 0.15$ sample at even higher fields up to 45 T.

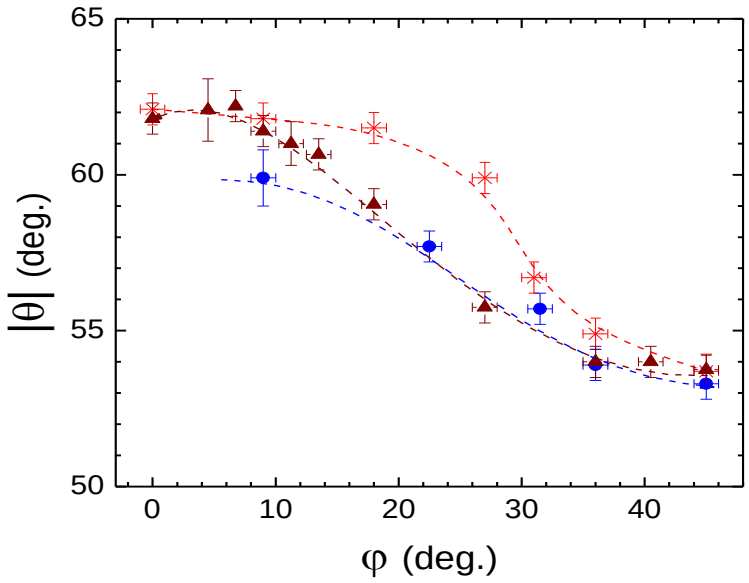

FIG. 5. Angular position $|\theta|$ of the AMRO features in the $R(\theta)$ curves plotted versus the azimuthal angle φ used in the $R(\theta)$ sweeps for $Nd_{2-x}Ce_xCuO_4$ single crystals with doping levels $x = 0.16$ (blue circles), 0.165 (brown triangles), and 0.17 (red stars). The dashed lines are guides to the eye.

SHUBNIKOV-DE HAAS (SDH) OSCILLATIONS

Motivated by the observation of AMRO suggesting magnetic breakdown in overdoped NCCO, we performed measurements in pulsed magnetic fields to search for multiple SdH frequencies. Fig. 6(a) shows the oscillating component of the interlayer magnetoresistance (normalized to the field-dependent background) for $x = 0.16$, 0.165, and 0.17. All the curves exhibit oscillations with two different frequencies. The slow oscillations, similar to those reported earlier for $x = 0.15$ and 0.16 [26], are associated with the small hole pockets of the reconstructed Fermi surface [see Fig. 1(c)]. The fast oscillations, shown on an enlarged scale in Fig. 6(b) have frequencies of about 11 kT. This is obviously consistent with the cross-sectional area of the large unreconstructed Fermi cylinder. The oscillation frequencies clearly depend on x. This dependence, plotted in Fig. 7 for both the slow and fast oscillations, rules out the possibility that the two frequencies are caused by a coexistence of two phases with different Fermi surfaces. Indeed, imagine a sample consisting of two phases with different carrier concentrations giving rise to different Fermi surface topologies. Then, a change of the nominal doping level x would lead to changing the volume fractions of the phases and, thus, affect the amplitudes of the SdH oscillations but not their frequencies. This

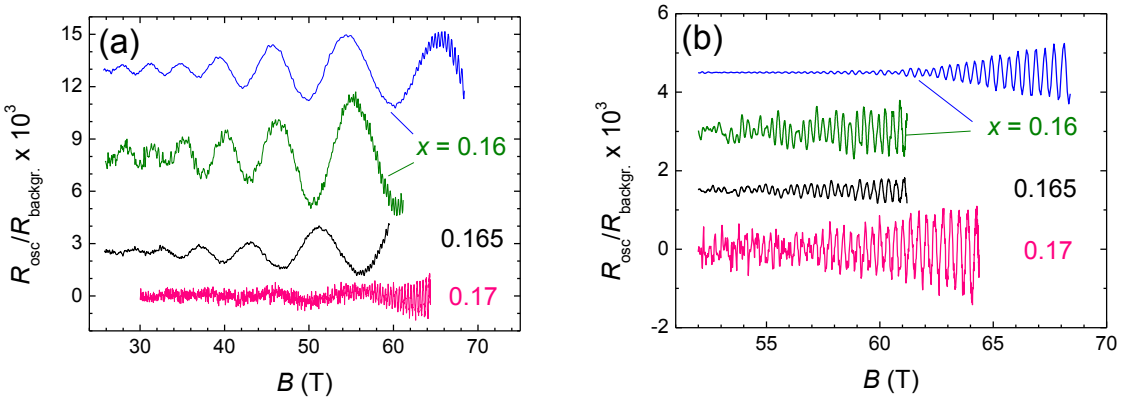

FIG. 6. (a) Oscillatory component of the interlayer magnetoresistance at pulsed fields applied perpendicular to the CuO_2 layers. The data was taken at $T = 2.5\,\mathrm{K}$ for $Nd_{2-x}Ce_xCuO_4$ single crystals with doping levels $x = 0.16$, 0.165, and 0.17, and for another sample with $x = 0.16$ at the Dresden and at the Toulouse (blue curve) high-field facilities, respectively. In addition to slow SdH oscillations, one can resolve fast oscillations emerging from $B \simeq 55\,\mathrm{T}$ for all three doping levels. (b) Fast SdH oscillations extracted from the data in (a) at $B > 54\,\mathrm{T}$ by filtering out the low-frequency component. The data in (a) and (b) are vertically shifted for better visibility

scenario obviously contradicts the regular x dependence of the oscillation frequencies shown in Fig. 7. Moreover, within our experimental resolution, the high frequency coincides with what is expected from the Luttinger rule for the given doping levels (solid line in Fig. 7). Thus, we conclude that both SdH frequencies are an inherent feature of each doping level in the range $x = 0.16 - 0.17$, rather than a result of a phase mixture. An important implication of this conclusion is that the Fermi surface remains reconstructed up to the highest doping level, $x = 0.17$, and the fast oscillations originate from magnetic breakdown through small gaps between the electron and hole pockets.

The SdH oscillations shown in Fig. 6 are very weak, $\sim 10^{-3}$ of the background resistance. To achieve the necessary resolution, we had to apply rather high currents of up to 10 mA. This caused considerable overheating which was estimated by recording $R(B)$ curves at low-field pulses for different currents and comparing them with steady-field data. On the other hand, one can see from Fig. 6(a) that the field dependence of the slow oscillations is not very steep: they can still be well resolved, at least for $x = 0.16$ and 0.165 at $B \sim 30 - 35\,\mathrm{T}$. Therefore, we have performed a SdH experiment in steady fields up to 35 T, which typically provide a lower noise level. Fig. 8(a) shows SdH oscillations for three doping levels recorded

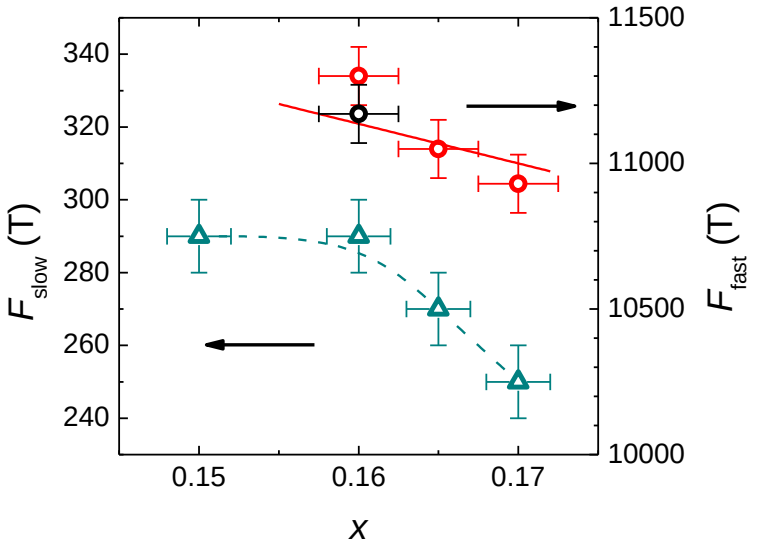

FIG. 7. Dependence of the frequency F of the slow (triangles, left-hand scale) and fast (circles, right-hand scale) oscillations on the doping level x. The $F_{\rm slow}$ data points summarize results obtained on several $Nd_{2-x}Ce_xCuO_4$ single crystals of each doping level in pulsed and steady fields. The dashed line is a guide to the eye. The $F_{\rm fast}(x)$ data points have been obtained in pulse-field experiments at the Dresden (red circles) and Toulouse (black circle) high-field facilities. The solid line shows the $F(x)$ dependence calculated from the nominal doping level according to the large Fermi surface shown in Fig. 1(b).

at steady fields with a transport current of 0.4 mA. This current was proved to cause no significant overheating effect ($\Delta T < 0.1$ K).

The oscillations frequencies, $F_{\rm slow} = 290$, 270, and 250 T for $x = 0.16$, 0.165, and 0.17, respectively, perfectly coincide with the pulsed field data. For $x = 0.17$, the oscillation amplitude barely exceeds the noise level even at the highest fields. However, for the other two compositions the slow oscillations can be observed down to below 20 T and are suitable for quantitative analysis.

By contrast to hole-underdoped $YBa_2Cu_3O_{6.5\pm\delta}$, for which several different low SdH frequencies have been reported [15, 16, 47], the present NCCO compound only shows a single frequency. In particular, so far we have not found any signature of oscillation beating, caused by a slight warping of the Fermi surface in the interlayer direction. This suggests that the distance between adjacent Landau levels, $\hbar\omega_c$ (where $\omega_c = eB/m_c$ is the cyclotron frequency and m_c is the relevant effective cyclotron mass), exceeds the interlayer dispersion

at fields $B \gtrsim 20\,\mathrm{T}$. Therefore, one should take into account the strong two-dimensionality of the system in the analysis of the oscillations. Generally speaking, the quasi-two-dimensional SdH effect is a very complex problem and has not yet received a comprehensive description even within the standard Fermi liquid theory [34, 48]. Moreover, it was recently pointed out [49] that the presence of strong electron correlations should dramatically affect the behavior of quantum oscillations, provided $\hbar\omega_c$ significantly exceeds the interlayer transfer integral $t_\perp$ and scattering-induced broadening of Landau levels $\sim \hbar/\tau$ (where τ is the scattering time). However, our case is simplified due to the weakness of the oscillation amplitude and the absence of higher harmonics, which is indicative of a strong Landau level broadening. Therefore, we adopt the so-called two-dimensional Lifshitz-Kosevich (LK) formula [50] for quantum oscillations in a two-dimensional metal with a constant chemical potential. It should be valid for the in-plane SdH effect, and we assume both the oscillating and monotonic components of the interlayer conductivity to be proportional to those of the in-plane conductivity. Then the field and temperature dependence of the oscillation amplitude are expressed as [50] $A_{\mathrm{osc}} \propto R_{\mathrm{T}} R_{\mathrm{D}} R_{\mathrm{MB}}$, where R_{T} and R_{D} are the standard temperature and Dingle reduction factors, respectively, and R_{MB} describes the influence of magnetic breakdown.[**?**]

From the T-dependence of the oscillation amplitude, given by $R_{\mathrm{T}} = (K\mu T/B)/\sinh(K\mu T/B)$ (where $K = 2\pi^2 k m_e/\hbar e \approx 14.69\,\mathrm{T/K}$, $\mu = m_c/m_e$ is the effective cyclotron mass normalized to the free electron mass m_e, k is the Boltzmann constant, and e is the elementary charge), one can estimate the effective cyclotron mass. Fig. 8(b) shows the experimental data for $x = 0.16$, fitted to the LK formula. From the steady-field data (circles) we derive $\mu_{0.16} = 0.92 \pm 0.05$. A similar value, $\mu_{0.165} = 0.9 \pm 0.05$, is obtained for $x = 0.165$. For comparison, the effective mass plot obtained from the pulsed-field data is shown by diamonds in Fig. 8(b), giving a somewhat lower value, $\mu_{0.16}^{\mathrm{pulse}} = 0.7 \pm 0.1$. The discrepancy is apparently caused by an uncertainty in the sample temperature in the pulse-field experiment. Although the induced eddy currents do not cause a significant heating effect due to the relatively long pulse duration, $\simeq 0.2\,\mathrm{s}$, the temperature is affected by the fast orientation of the paramagnetic Nd^{3+} ions reducing the entropy of the spin system. Obviously, the effect is enhanced at lower temperatures, which results in a flatter apparent T-dependence and, hence, in a smaller μ. Therefore, the derivation of the cyclotron mass from the steady-field data is considered more reliable. Unfortunately, the fast oscillations have so far been detected only

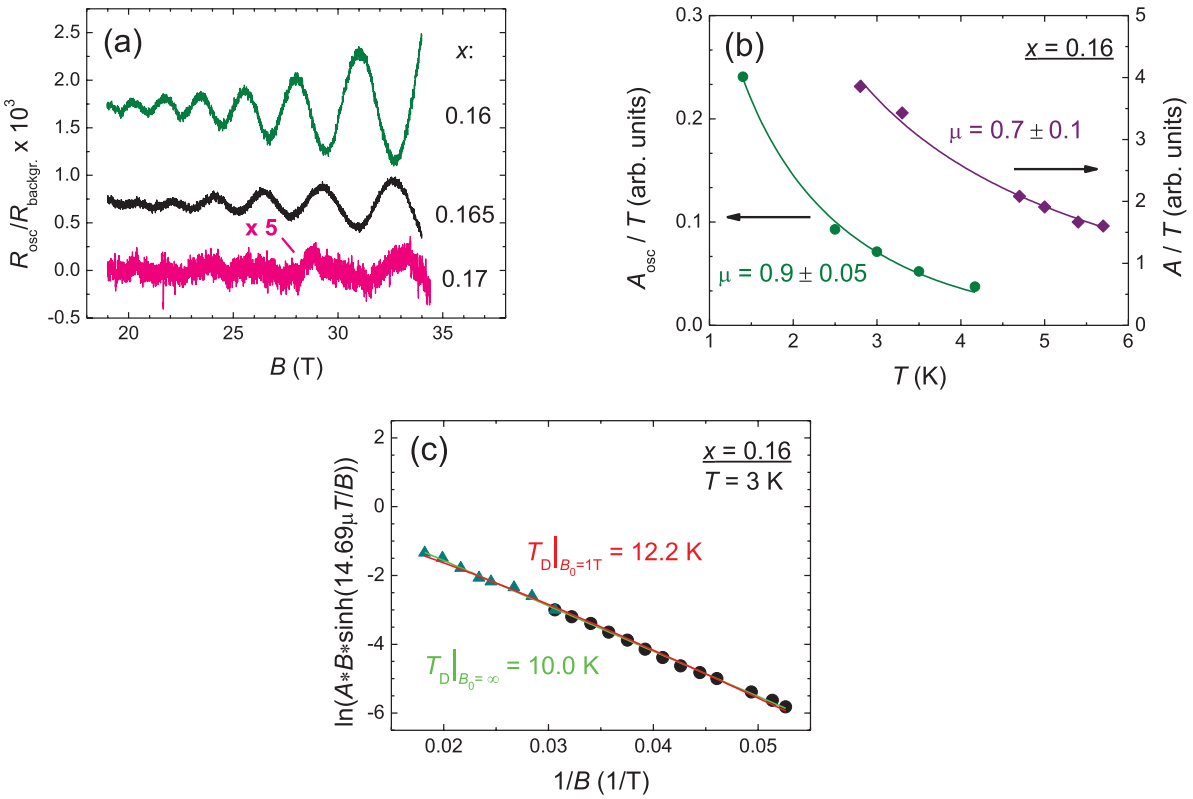

FIG. 8. (a) Slow SdH oscillations in overdoped $Nd_{2-x}Ce_xCuO_4$ single crystals recorded in steady magnetic fields at $T = 1.5$ K. The data are vertically shifted for better visibility. (b) Temperature dependence of the oscillation amplitude A_{osc} obtained from the steady-field (circles) and pulsed-field (diamonds) experiments. Solid lines are Lifshitz-Kosevich fits yielding the effective cyclotron mass values $\mu \approx 0.9$ and 0.7 for the steady- and pulsed-field data, respectively, see text. (c) Dingle plot for the slow-oscillation amplitude including pulsed- (triangles) and steady-(circles) field data. The fits to the theoretical field dependence assuming a magnetic breakdown field $B_0 = \infty$ (green line) and 1 T (red line) are almost indistinguishable and give just slightly different values for the Dingle temperature, see text.

in pulsed fields above 50 T. The estimate of the cyclotron mass from this pulse-field data yields $\mu = 2.2 \pm 0.2$ for $x = 0.17$ and 2.4 ± 0.2 for $x = 0.165$. We should, however, keep in mind that the real values may be about 20% higher.

After having derived the cyclotron mass, we can use the field dependence of the oscillation amplitude to estimate the Dingle temperature, T_D, determined by the scattering-induced broadening of Landau levels. The corresponding Dingle plot for $x = 0.16$ is shown

in Fig. 8(c), yielding $T_D \approx 10\,K$. Strictly speaking, when fitting the B-dependent SdH amplitude we should take into account the effect of magnetic breakdown through the gap (which is thus considered as a breakdown junction) between the hole and electron pockets of the reconstructed Brillouin zone. The closed orbit on the small hole pocket responsible for the slow oscillations involves reflections from two breakdown junctions. Therefore, the corresponding damping factor for the oscillation amplitude is [50, 51]: $R_{MB}^{slow} = [1-\exp(-B_0/B)]$, where B_0 is the characteristic breakdown field. Including R_{MB} with a very low breakdown field, $B_0 = 1\,T$, (see below) into the field dependence $A_{osc}(B)$, we obtain the fit shown by the red line in Fig. 8(c), which is almost indistinguishable from the pure [$B_0 = \infty$, green line in Fig. 8(c)] Dingle fit and gives just a slightly different $T_D \approx 12\,K$. Using the conventional relationship between T_D and the scattering time τ, $T_D = \hbar/2\pi k_B\tau$, we estimate $\tau \approx 0.15\,ps$. This corresponds to a mean-free path averaged over the cyclotron orbit of $\langle\ell\rangle \simeq 18\,nm$.

The obtained cyclotron mass and scattering time values determine the field strength parameter $\omega_c\tau$ which merely reaches unity at $B \simeq 35\,T$ (for the slow oscillations; for the fast SdH oscillations it is even lower due to heavier m_c). This justifies the validity of the standard two-dimensional LK formula for fitting the steady field data. However, as mentioned above, one can expect deviations from the LK theory at higher fields, when $\omega_c\tau > 1$. In particular, in future it would be interesting to discuss the pulsed field data in terms of the recent theory [49] taking into account strong electron interactions.

As follows from the comparison between the two fits in Fig. 8(c), it is very difficult to extract the breakdown field from the B-dependence of the slow oscillation amplitude in the given restricted field range. For the fast oscillations, the breakdown reduction factor is determined by tunneling through 8 equivalent magnetic breakdown junctions and has the form [50, 51]: $R_{MB}^{fast} = \exp(-4B_0/B)$. One can see that it has exactly the same functional field dependence as the Dingle factor, $R_D = \exp(-K\mu T_D/B)$, which makes it impossible to evaluate T_D and B_0 separately. Nevertheless, we can make a rough estimate by simply comparing the amplitudes of the fast and slow oscillations at a given field, say, $B = 60\,T$. Assuming the same Dingle temperature for the carriers on the small and large orbits and using the cyclotron mass values $\mu_{slow} = 0.9$ and $\mu_{fast} = 2.2$, we can reproduce the ratio between the oscillation amplitudes, $A_{slow}/A_{fast} \simeq 10$ observed for $x = 0.16$ and 0.165 (see Fig. 6) by taking $B_0 = 7$ T. For the highest doping level, $x = 0.17$, the slow and fast oscillations have approximately equal amplitudes at 60 T, yielding $B_0 \simeq 1\,T$. This estimate

demonstrates that observation of both the high and low frequencies in the SdH spectrum is only possible at $B \gg B_0$, i.e. in the strong magnetic-breakdown limit. This is because the strong difference in the Dingle factors for the slow and fast oscillations, originating from different cyclotron masses and the large Dingle temperature, must be compensated by the difference in the magnetic-breakdown reduction factors. In particular, for $x = 0.17$ the ratio between the breakdown factors at 60 T is: $R_{\rm MB}^{\rm fast}/R_{\rm MB}^{\rm slow} \simeq 60$.

Here, it is worth making a remark concerning the contribution of the electron pockets of the reconstructed Fermi surface [see Fig. 1(c)] to the SdH effect. In the strong magnetic breakdown regime, $B \gg B_0$, the probability of encircling a full closed orbit around an electron pocket, involving reflections at 4 breakdown junctions, is strongly suppressed. Taking the above estimate, $B_0 = 7\,\mathrm{T}$ for $x = 0.16$, we arrive at the breakdown reduction factor $R_{\rm MB}^{\rm el.\,pocket} = [1 - \exp(-B_0/B)]^2 \approx 10^{-2}$ at $B = 60\,\mathrm{T}$, which is $\simeq 10$ times smaller than for the oscillations from the small hole pockets at the same field (we recall that the latter require only two reflections from magnetic breakdown junctions). Additional damping comes from the temperature and Dingle factors, since the cyclotron mass corresponding to the electron orbits is, obviously, heavier than that of the small hole orbits. Altogether, we expect the amplitude of the oscillations coming from the electron pockets to be about two orders of magnitude lower than that associated with the hole pockets at $x = 0.16$ and even further reduced at higher doping levels. It is, therefore, not surprising that no clear signature of the electron pockets has been found in the SdH spectrum so far.

Using the Blount criterion, one can estimate the energy gap Δ between the electron and hole bands formed by the superlattice potential [52]: $\Delta \simeq (\hbar e B_0 \varepsilon_{\rm F}/m_{\rm c})^{1/2}$, where $\varepsilon_{\rm F} \approx 0.5\,\mathrm{eV}$ is the Fermi energy and $m_{\rm c} \approx 2.2 m_{\rm e}$ is the cyclotron mass corresponding to the large magnetic-breakdown orbit. With the above values B_0, one obtains $\Delta \simeq 14\,\mathrm{meV}$ for $x = 0.16$ and 5 meV for $x = 0.17$. While this is, of course, only a rough estimate, it shows that the superlattice energy gap is very small, namely in the meV range.

CONCLUDING REMARKS AND OUTLOOK

The experimental results presented here for high-quality overdoped $Nd_{2-x}Ce_xCuO_4$ single crystals provide convincing evidence for the presence of magnetic breakdown. This indicates that the Fermi surface is reconstructed up to the highest doping level ($x = 0.17$) reliably

attainable for bulk NCCO. Note that this doping level corresponds to the very end of the superconducting range in the phase diagram: T_c extrapolates to zero at $x \approx 0.175$ [41]. Furthermore, our data show that the superlattice potential is strongly reduced at the highest doping level. Therefore, it is likely that both the superlattice potential and superconductivity vanish at the same carrier concentration. This would strongly suggest a close relation between the two ordering phenomena.

The existence of the superlattice potential in the overdoped regime distinguishes our electron-doped compound from the hole-doped cuprates. In the latter, a broken symmetry has been observed only below optimal doping so far. The mechanism responsible for the broken translational symmetry is still to be clarified. One possibility is that the commensurate antiferromagnetic ordering persists from the underdoped regime [53, 54]. It was very recently proposed [55] that, by contrast to hole-doped cuprates, the mechanism underlying the metal-insulator transition in the electron-doped materials is of magnetic origin rather than due to electronic correlations. In this case the metallic and superconducting state could coexist with antiferromagnetism, provided the magnetic interaction is not strong enough for causing a metal-insulator transition. However, until now no static magnetic ordering has been detected in overdoped NCCO [56]. This seems to favor another scenario associated with a "hidden" d-density-wave ordering [17, 57]. On the other hand, it is possible that the ordering only exists at high magnetic fields, i.e. at the conditions of our present experiment. An in-depth study of the magnetic properties at high fields should elucidate this issue.

Although our experiments already give new and interesting insight, further detailed Fermi surface studies in high fields are highly important for clarifying the origin of the superlattice potential. Angle-dependent magnetoresistance experiments extending up to the highest steady fields of 45 T and covering also a broader doping range, should allow a quantitative characterization of the Fermi surface geometry and its dependence on the carrier concentration. The angle dependence of the SdH oscillations is also potentially important for understanding the spin state of the conduction electrons and the nature of the ordering [15, 16, 58].

As mentioned above, the suggested reconstruction of the Fermi surface in overdoped NCCO implies the existence of electron pockets, in addition to the hole ones. However, the magnetic breakdown occurring at the highest doping levels suppresses orbits encircling the whole electron pocket more effectively than those around hole pockets. Therefore, lower doping levels with a stronger superlattice potential appear to be more appropriate for searching

for a manifestation of the electron pockets in high-field magnetotransport.

Another still open question is how the Fermi surface develops upon entering the underdoped range of the phase diagram. The lowest doping level at which we have so far succeeded in finding SdH oscillations is $x = 0.15$. The reason why they are not observed at lower doping is not clear. Could it be that the closed hole pockets disappear immediately below the optimal doping? Or is it because the conventional orbital effect on the interlayer conductivity becomes too small, compared to the emerging anomalous incoherent magnetotransport? In the latter case, it might be more convenient to look for magnetic quantum oscillations in the in-plane resistivity or in thermodynamic properties. Unfortunately, the oscillations of magnetization (de Haas–van Alphen effect) can hardly be detected in NCCO due to an overwhelming magnetic contribution from the Nd^{3+} moments. One could, however, search for the oscillations in some other properties such as sound velocity or magnetostriction.

Acknowledgments

The work was supported by EuroMagNET II under the EU contract 228043, by the Deutsche Forschungsgemeinschaft via the Research Unit FOR 538 and grant GR 1132/15, and by the German Excellence Initiative via the Nanosystems Initiative Munich.

REFERENCES

* Mark.Kartsovnik@wmi.badw.de

[1] Cracknell A P and Wong A C 1973 *The Fermi Surface* (London: Oxford University Press)

[2] Ashcroft N W and Mermin N D 1976 *Solid State Physics* (Philadelphia: Saunders College)

[3] Hussey N E, Abdel-Jawad M, Carrington A, Mackenzie A P, Balicas L 2003 *Nature* **425** 814

[4] Abdel-Jawad M, Balicas A C, Balicas L, Kennet M P, Mackenzie M P, McKenzie R H and Hussey N E 2006 *Nature Phys.* **2** 821

[5] Doiron-Leyraud N, Proust C, LeBoeuf D, Levallois J, Bonnemaison J B, Liang R, Bonn D A, Hardy W N and Taillefer L 2007 *Nature* **447** 565

[6] Yelland E A, Singleton J, Mielke C H, Harrison N, Balakirev F F, Dabrowski B and Cooper J R 2008 *Phys. Rev. Lett.* **100** 047003

[7] Bangura A F, Fletcher J D, Carrington A, Levallois J, Nardone M, Vignolle B, Doiron-Leyraud N, LeBoeuf D, Taillefer L, Adachi S, Proust C and Hussey N E 2008 *Phys. Rev. Lett.* **100** 047004

[8] Vignolle B, Carrington A, Cooper R A, French M M J, Mackenzie A P, Jaudet C, Vignolles D, Proust C and Hussey N E 2008 *Nature* **455** 952

[9] Andersen O K, Liechtenstein A I, Jepsen O and Paulsen N 1995 *J. Phys. Chem. Solids* **56** 1573

[10] Singh D J and Pickett W E 1992 *Physica C* **203** 193

[11] Platé M, Mottershead J D , Elfimov I S, Peets D C, Liang R, Bonn D A, Hardy W N, Chiuzbaian S, Falub M, Shi M, Patthey L and Damascelli A 2005 *Phys. Rev. Lett.* **95** 077001

[12] Sebastian S E, Harrison N, Palm E and Murphy T P, Mielke C H, Liang R, Bonn D A, Hardy W N and Lonzarich G G 2008 *Nature* **454** 200

[13] Jaudet C, Vignolles D, Audouard A, Levallois J, LeBoeuf D, Doiron-Leyraud N, Vignolle B, Nardone M, Zitouni A, Liang R, Bonn D A, Hardy W N, Taillefer L and Proust C 2008 *Phys. Rev. Lett.* **100** 187005

[14] Damascelli A, Hussain Z and Shen Z X 2003 *Rev. Mod. Phys.* **75** 473

[15] Sebastian S E, Harrison N, Goddard P A, Altarawneh M M, Mielke C H, Liang R, Bonn D A, Hardy W N, Andersen O K and Lonzarich G G 2010 *Phys. Rev. B* **81** 214524

[16] Ramshaw B J, Vignolle B, Day J, Liang R, Hardy W N, Proust C and Bonn D A 2011 *Nature Phys.* **7** 234

[17] Jia X, Goswami P and Chakravarty S 2009 Phys. Rev. B **80** 134503

[18] Lee P A 2008 Rep. Prog. Phys. **71** 012501

[19] Millis A J and Norman M R 2007 *Phys. Rev. B* **76** 220503(R)

[20] LeBoeuf D, Doiron-Leyraud D, Levallois J, Daou R, Bonnemaison J B, Hussey N E, Balicasand L, Ramshaw B J, Liang R, Bonn D A, Hardy W N, Adachi S, Proust C and Taillefer L 2007 *Nature* **450** 533

[21] Kaul R K, Kim Y B, Sachdev S and Senthil T 2008 *Nature Phys.* **4** 28

[22] Dimov I, Goswami P, Jia X and Chakravarty S 2008 *Phys. Rev. B* **78** 134529

[23] Alexandrov A S 2008 *J. Phys. Condens. Matter* **20** 192202

[24] Varma C M 2009 *Phys. Rev. B* **79** 085110

[25] Pereg-Barnea T, Weber H, Refael G and Franz M 2010 *Nature Phys.* **6** 44

[26] Helm T, Kartsovnik M V, Bartkowiak M, Bittner N, Lambacher M, Erb A, Wosnitza J and Gross R 2009 *Phys. Rev. Lett.* **103** 157002

[27] Massidda S, Hamada N, Yu J, Freeman A J 1989 *Physica C* **157** 571

[28] Armitage P N, Ronning F, Lu D H, Kim C, Damascelli A, Shen K M, Feng D L, Eisaki S, Shen Z X, Mang P K, Kaneko N, Greven M, Onose Y, Taguchi Y and Tokura Y 2002 *Phys. Rev. Lett.* **88** 257001

[29] Matsui H, Takahashi T, Sato T, Terashima K, Ding H, Uefuji T and Yamada K 2007 *Phys. Rev. B* **75** 224514

[30] Lambacher M, Ph.D. thesis, Technische Universität München, 2008

[31] Dagan Y, Qazilbash M M, Hill C P, Kulkarni V N and Greene R L 2004 *Phys. Rev. Lett.* **92** 167001

[32] Eun J, Jia X and Chakravarty S 2010 *Phys. Rev. B* **82** 094515

[33] Kusko C, Markiewicz R S, Lindroos M and Bansil A 2002 *Phys. Rev. B* **66** 140513(R)

[34] Kartsovnik M V 2004 *Chem. Rev.* **104** 5737

[35] Bergemann C, Mackenzie A P, Julian S R, Forsythe D and Ohmichi E 2003 *Adv. Phys.* **52** 639

[36] Baxendale M, Mordkovich V Z and Yoshimura S 1998 *Solid State Commun.* **107** 165

[37] Yamaji K 1989 *J. Phys. Soc. Jpn.* **58** 1520

[38] Kartsovnik M V, Laukhin V N, Pesotskii S I, Schegolev I F and Yakovenko V M 1992 *J. Phys. I France* **2** 89

[39] Grigoriev P D 2010 *Phys. Rev. B* **81** 205122

[40] Helm T, Kartsovnik M V, Sheikin I, Bartkowiak M, Wolff-Fabris F, Bittner N, Biberacher W, Lambacher M, Erb A, Wosnitza J and Gross R 2010 *Phys. Rev. Lett.* **105** 247002

[41] Lambacher M, Helm T, Kartsovnik M V and Erb A 2010 *Eur. Phys. J. Special Topics* **188** 61

[42] Kurihara Y 1992 *J. Phys. Soc. Jpn.* **61** 975

[43] Kartsovnik M V, Grigoriev P D, Biberacher W and Kushch N D 2009 *Phys. Rev. B* **79** 165120

[44] Yu W, Higgins J S, Bach P and Greene R L 2007 *Phys. Rev. B* **76** 020503(R)

[45] Wu T, Wang C H, Wu G, Fang D F, Luo J L, Liu G T and Chen X H 2008 *J. Phys.: Condens. Matter* **20** 275226

[46] Analytis J G, Abdel-Jawad M, Balicas L., French M M J, and Hussey N E 2007 *Phys. Rev. B* **76** 104523

[47] Audouard A, Jaudet C, Vignolles D, Liang R, Bonn D A, Hardy W N, Taillefer L and Proust C 2009 *Phys. Rev. Lett.* **103** 157003

[48] Grigoriev P D 2003 *Phys. Rev. B* **67** 144401

[49] Thompson L and Stamp P C E 2010 *Phys. Rev. B* **81** 100514(R)

[50] Shoenberg D 1984 *Magnetic Oscillations in Metals* (Cambridge: Cambridge University Press)

[51] Falicov L M and Stachowiak H 1966 *Phys. Rev.* **147** 505

[52] Blount E I 1962 *Phys. Rev.* **126** 1636

[53] Das T, Markiewicz R S and Bansil A 2008 *J. Phys. Chem. Solids* **69** 2963

[54] Sachdev S 2010 *Phys. Stat. Sol. B* **247** 537

[55] Weber C, Haule K and Kotliar G 2010 *Nature Phys.* **6** 574

[56] Motoyama E M, Yu G, Vishik I M, Vajk O P, Mang P K and Greven M 2007 *Nature* **445** 186

[57] Chakravarty S, Laughlin R B, Morr D K and Nayak C 2001 *Phys. Rev. B* **63** 094503

[58] Garcia-Aldea D and Chakravarty S 2010 *Phys. Rev. B* **82** 184526